Author/s:
Talodthaisong, C;Boonta, W;Thammawithan, S;Patramanon, R;Kamonsutthipaijit, N;Hutchison, JA;Kulchat, S

Title:
Composite guar gum-silver nanoparticle hydrogels as self-healing, injectable, and antibacterial biomaterials

Date:
2020-09-01

Citation:
Talodthaisong, C., Boonta, W., Thammawithan, S., Patramanon, R., Kamonsutthipaijit, N., Hutchison, J. A. & Kulchat, S. (2020). Composite guar gum-silver nanoparticle hydrogels as self-healing, injectable, and antibacterial biomaterials. Materials Today Communications, 24, https://doi.org/10.1016/j.mtcomm.2020.100992.

Persistent Link:
https://hdl.handle.net/11343/344920

Composite guar gum-silver nanoparticle hydrogels as self-healing, injectable, and antibacterial biomaterials

Chanon Talodthaisong[a], Wissuta Boonta[a], Saengrawee Thammawithan[b], Rina Patramanon[b], Nuntaporn Kamonsutthipaijit[c], James A. Hutchison[d], Sirinan Kulchat[a]*

[a]*Materials Chemistry Research Center, Department of Chemistry and Center of Excellence for Innovation in Chemistry, Faculty of Science, Khon Kaen University, Khon Kaen, 40002, Thailand.*

[b]*Department of Biochemistry, Faculty of Science, Khon Kaen University, Khon Kaen, 40002, Thailand.*

[c]*Synchrotron Light Research Institute (Public Organization) 111 University Avenue, Muang District, Nakorn Ratchasima 30000, Thailand.*

[d]*School of Chemistry, The University of Melbourne, Parkville, Victoria 3010, Australia.*

**Email*: sirikul@kku.ac.th

Keywords: Self-healing, Curcumin, Borate, Natural Gum, Antimicrobial

Abstract

Biomaterial-based hydrogels incorporating antibacterial agents may provide sustainable solutions to biomedical device failures and the prevention of infections. Herein we report guar gum hydrogels, cross-linked with borax and loaded with silver nanoparticles, that are injectable, exhibit rapid self-healing, and show antibacterial properties towards both gram-positive and gram-negative bacteria. The hydrogels are fully characterized by infrared spectroscopy, thermogravimetric analysis, scanning electron microscopy, and rheological measurements. An important focus was to minimize borax content, thus reducing the toxicity of the gels greatly, whilst retaining their favorable viscoelastic properties. When the low borax-content hydrogels are composited with curcumin-stabilized silver nanoparticles, the hydrogels show activity against *Escherichia coli (E. coli)*, *Pseudomonas aeruginosa (P. aeruginosa)*, and *Staphylococcus aureus (S. aureus)*.

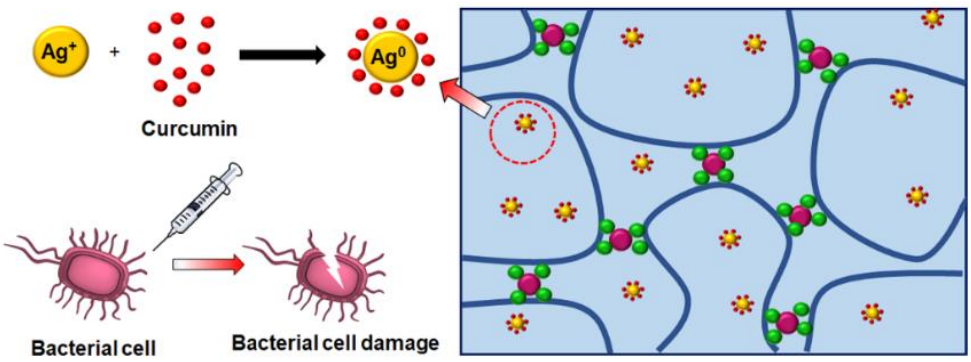

Graphical Abstract

1. Introduction

Hydrogels are three-dimensional polymeric networks that absorb a large amount of water [1,2]. They are soft and wet materials in which both chemical and physical gelling can coexist [1]. Their ability to retain water, along with their other biomimetic properties, make them of interest in medical [1,3] sensor [4], cosmetic [5], materials science [6], tissue engineering [7,8] and pharmaceutical [9,10] applications. Hydrogels with dynamically cross-linked polymer networks also have promising potential as self-healing materials [11]. These materials are dynamic at the molecular level due to reversible covalent bonding based on the constitutional dynamic chemistry concept. Self-healing hydrogels can automatically repair their function after damage and can be based on either reversible covalent or non-covalent crosslinked gel networks [12]. Nevertheless, self-healing hydrogels can have limitations, including slow speeds of self-healing, costly synthesis of macromolecular components, and complications during chemical modification [13,14]. In addition, the present focus on environmental sustainability demands that these materials be produced from natural (renewable) resources.

Guar Gum (GG) is an excellent starting biomaterial for modified polymers. The guar gum extracted from the seeds of *Cyamopsis tetragonoloba* consists of a (1,4)-linked *β*-D-mannopyranose main chain with a branched α-D-galactopyranose unit at the 6-position [15]. It is popular in biological applications and the food industry because it is non-toxic, cheap, biodegradable, and easily forms gels in water at room temperature [16,17]. In this work, borax was used as a cross-linker of GG because the dynamic nature of the boronate ester linkages imparts the gel with self-healing properties without any external stimuli [16].

The incorporation of metallic nanoparticles into materials can endow them with unique optical, electronic and biomedical properties [18-22]. Incorporation of silver nanoparticles (AgNPs) into hydrogels has been shown to modify gelation and lead to antimicrobial activity [23-25]. Hydrogel-AgNPs composites thus have potential as injectable materials for use in antimicrobial pharmaceutical formulations [26]. Herein we fabricate AgNPs using curcumin (1,7-bis(4-hydroxy-3-methoxy phenyl)-1,6 heptadiene-3,5-diene), the principal curcuminoid of turmeric, as both reductant and stabilizing ligand. Curcumin is known for its own various biological activities [27], but is poorly soluble in water, restricting its usefulness in biomedical applications. Here however, the curcumin-stabilized silver nanoparticles are easily dispersed in water and combined efficiently within our hydrogels.

In the final part of this work, we test the structural properties of the curcumin AgNP-incorporated GG-borax hydrogels and assess their anti-microbial properties against a range of

bacteria. The composite AgNPs hydrogel is shown to have better swelling properties than neat GG-borax hydrogels, to be self-healing, injectable by syringe, and highly resistant to various bacteria, suggesting future potential in the realm of biomedicine (e.g. wound healing, drug delivery). This work is part of a continuing drive in our laboratories to exploit natural products and to expand their technological usefulness by chemical and nanoscale modifications.

2. Experimental

2.1 Materials

Guar gum was purchased from Chemipan Corporation Co. , Ltd, Thailand. Sodium Hydroxide (99%) was purchased from RCL Labscan. Borax (di-sodium tetraboratedecahydrate) was purchased from QRëC, New Zealand. Silver nitrate was purchased from POCH™ and Curcumin synthetic grade (pure > 97%) was purchased from TCI, Europe. Deionized water (DI) with specific resistivity of 18.2 MΩ.cm was obtained from a RiO_s^{TM} Type I Simplicity 185 (Millipore water purification system). Dimethylsulfoxide (DMSO) was purchased from Riedel-deHaën®, Germany. K_2CO_3 was purchased from Merck, Germany. Ethanol was obtained from Merck, Germany. Bacterial strains were obtained from the Biochemistry Laboratory, Biochemistry Department, Faculty of Science, Khon Kaen University, Thailand. Antimicrobial activity assays used *Escherichia coli* (*E. coli* O157H7), *Pseudomonas aeruginosa* (*P. aeruginosa* ATCC27853), and *Staphylococcus aureus* (*S. aureus* ATCC25923).

2.2. Guar gum purification procedure

Guar gum was purified according to a literature method [28]. Briefly, crude guar gum (10 g) was stirred in 800 mL of DI water at room temperature for 12 hr. The guar gum solution was then centrifuged at 5000 rpm for 20 min (12 mL x 66 tubes), retaining the supernatant liquid. The supernatant was then precipitated with 400 mL ethanol and centrifuged at 5000 rpm for 5 min. The white solid material thus obtained was washed again with ethanol followed by DI water. The material was then freeze-dried to obtain the purified guar gum powder.

2.3. Preparation of borax cross-linked guar gum hydrogels and guar gum films

The borax cross-linked guar gum hydrogels were prepared via a modification of a previous report [16]. Briefly, the solution of guar gum was prepared using purified guar gum powder (0.1 g) in 20 mL of DI water, stirred for 1 hr at room temperature. The solution pH was then adjusted to 8 by 0.1 M NaOH (200 μL). The borax solutions were prepared in different proportions in 10 mL of DI water (i.e. 2, 4, 6, and 8 wt% of borax). 500 μL of the prepared borax solution was then added to the guar gum solution to give final gelation solutions containing 0.5 wt% GG and 0.05 wt%, 0.1 wt%, 0.14 wt% and 0.2 wt% borax (10:1, 5:1, 3.6:1, and 2.5:1 GG:borax weight ratio respectively). The series of four hydrogels thus obtained were designated here GG-1, GG-2, GG-3 and GG-4, respectively (Table S1). For the film preparation, the obtained hydrogel was poured into a petri dish then dried in an oven at 40 ^{o}C for 24 hr. DI water was then poured over the whole film area, and the dish let sit until the film was swollen. Finally, the film was removed from the petri dish and put on a plastic plate to dry at room temperature.

2.4. Synthesis of curcumin-stabilized silver nanoparticles (Cur-AgNPs)

A solution of 20 mM curcumin in DMSO (250 μl) was added to 22.5 mL of DI water in a 100 mL round bottom flask. The solution pH was then adjusted to 10 by 0.07 M K_2CO_3 and the solution heated up to 100 °C. Next, 2.5 mL of 10 mM $AgNO_3$ was quickly added to the solution mixture. The mixture was stirred vigorously at 100 °C for 1 hr and filtered by micro filter to obtain the Cur-AgNPs [29]. The concentration of Cur-AgNPs was estimated to be 3.14 nM based on an extinction coefficient of 41.8 x 10^8 $M^{-1}.cm^{-1}$ at 407 nm for 17.7 nm diameter citrate-silver nanoparticles [30].

2.5 Preparation of GG-2/Cur-AgNPs hydrogel

Purified guar gum (0.1 g) was stirred in 20 mL of the Cur-AgNPs solution Cur-AgNPs at concentrations of 0.20, 0.39, 0.78, 1.57, and 3.14 nM, with 0.1 M NaOH (200 μL) and 4 wt% borax (500 μL) then added to each solution (Table S2). The mixture was then stirred until gelation occurred, affording slightly yellow hydrogels designated GG-2/Cur-AgNPs 0.20 nM, GG-2/Cur-AgNPs 0.39 nM, GG-2/Cur-AgNPs 0.78 nM, GG-2/Cur-AgNPs 1.57 nM, and GG-2/Cur-AgNPs 3.14 nM, respectively.

2.6 Characterization

2.6.1 Characterization of hydrogels

2.6.1.1 ATR-FTIR spectroscopy

The ATR-FTIR spectra of guar gum and borax cross-linked hydrogels were recorded in the solid state by an Attenuated Total Reflection Fourier Transform Infrared spectrophotometer using a standard Pike ATR cell (Model: Bruker TENSOR 27, Netherland) in the range 4000-600 cm^{-1}.

2.6.1.2 Surface morphology studies

Surface morphology of guar gum powder, GG-2 hydrogel films and freeze-dried GG-2 hydrogels were analyzed by scanning electron microscopy (Model: 1450VP, LEO, USA). Freeze-dried GG-1, GG-2, GG-3, and GG-4 hydrogels were characterized by digital microscopy (Model: Leica DVM6, Singapore).

2.6.1.3 Thermal studies

The thermogravimetric analysis (TGA, Rigaku TG-8120) of guar gum and cross-linked hydrogels was carried out under a nitrogen atmosphere from 25 ºC to 800 ºC with a heating rate of 10 ºC/min.

2.6.1.4 Viscosity studies

The viscoelastic properties of the cross-linked hydrogels were analyzed using a Brookfield viscometer Model RVDV-II+, USA.

2.6.1.5 Rheological studies

The rheological properties of the cross-linked hydrogels were examined using a parallel-plate (smooth stainless steel, 25 mm diameter) rheometer (Physica MCR500, Germany). The G′ (storage modulus) and G″ (loss modulus) of the hydrogels were further monitored by strain amplitude (γ_0) under strain from 0.1% to 100% at a constant temperature (25 ºC) and frequency (1 rad s^{-1}). For angular frequency sweep experiments, G′ and G″ were measured under an angular frequency range from 1 to 100 rad s^{-1} and with strain fixed at 1%.

2.6.2 Characterization of Cur-AgNPs

2.6.2.1 Optical properties

The optical properties of the as-prepared Cur-AgNPs in DI water were characterized by UV-Vis spectroscopy (Model: Agilent 8453, USA) using 1.0 cm quartz cells in the range of 200-700 nm.

2.6.2.2 Morphology and particle size studies by TEM

Morphology of Cur-AgNPs was determined by transmission electron microscopy (Model: Tecnai G^2-20 FEI, Netherland) under an accelerating voltage of 200 kV. A sample volume of 10 μL of Cur-AgNPs was dropped on a copper grid (300 mesh), then dried at room temperature before measurements. The size distribution was calculated using the ImageJ program.

2.6.2.3 Dynamic light scattering (DLS)

Dynamic light scattering, used to determine the size distribution of the Cur-AgNPs in solution, was undertaken using a Malvern Zetasizer Nano series (Nano ZS, UK).

2.6.2.4 Particle size and size distribution studies by SAXS technique

The particle size and size distribution of Cur-AgNPs were also characterized by the Small Angle X-ray Scattering (SAXS) technique. The experiments were measured using a multipole wiggler source on Beamline 1.3W (BL1.3W:SAXS) of the Synchrotron Light Research Institute (SLRI), Thailand. A MarCCD Rayonix SX165 detector with a sample-to-detector distance of 4439 mm was used and the samples were exposed to X-ray emission (λ = 1.38 Å) at room temperature for 10 min. A sample volume of 60 μL was used. Background subtraction was carried out using pure water. The 2D SAXS images were reduced and radially averaged by in-house software at SLRI (SAXSIT), to obtain 1D scattering curves. The unified exponential-power law model of Beaucage was used to fit the 1D scattering curves, where the scattering intensity is given by (1) [31]:

$$I(q) = G\exp\left(-\frac{q^2R_g^2}{3}\right) + B\left(\left[erf\left(\frac{qR_g}{\sqrt{6}}\right)\right]^3/q\right)^P \quad (1)$$

The prefactors G and B, the radius of gyration (R_g), and the exponent P, are fit parameters. The fitting was carried out with a least-squares minimization procedure using the software package SASfit [32].

To investigate the particle size and size distribution, the lognormal distribution of the particle size is assumed where the lognormal distribution function, $f(R)$ is given by (2) [33-34]:

$$f(R) = \frac{1}{R\sigma(2\pi)^{\frac{1}{2}}} exp\left\{-\frac{\left[log\left(\frac{R}{m}\right)\right]^2}{2\sigma^2}\right\} \quad (2)$$

Where R is the particle size and $f(R)$ is the number distribution. The mean particle radius, $\langle R \rangle$ and the standard deviation of the particle size, *SD*, which can be obtained from the lognormal distribution, are related to m and σ by (3):

$$\langle R \rangle = m \exp\left(\frac{\sigma^2}{2}\right) \text{ and } SD = m\sqrt{\omega(\omega - 1)} \quad (3)$$

where $\omega = \exp(\sigma^2)$. The two parameters, m and σ, of the lognormal distribution can be obtained in terms of the ratio B/G and R_g of the SAXS scattering profile [33]. This allows us to extract the particle size and distribution information from the fit of the unified model of Beaucage. The parameters m and σ can be obtained directly by (4):

$$m = \{5R_g^2/[3\exp(14\sigma^2)]\}^{1/2} \text{ and } \sigma = \left\{\frac{\ln[BR_g^4/(1.62G)]}{12}\right\}^{1/2} \quad (4)$$

2.7 Water absorption measurements

The degree of swelling of the hydrogels was studied in DI water at room temperature. 0.1 g of each GG hydrogel film was soaked in 50 mL water for a prescribed time, then removed with excess water dabbed away using filter paper. The gels were then weighed until a constant weight was obtained. The swelling degree was calculated using:

$$Swelling\ degree = ((W_s - W_o) / W_o) \times 100 \quad (5)$$

Where W_s is the swollen weight of the soaked hydrogel and W_o is original weight of the dry hydrogel. All experiments were done in triplicate.

2.8 Antimicrobial activity

The antimicrobial activities of the GG-2/Cur-AgNP hydrogels were evaluated against pathogenic bacteria *E.coli* (Gram-negative bacteria), *P. aeruginosa* (Gram-negative bacteria) and *S. aureus* (Gram-positive bacteria). The antimicrobial activity was carried out over 24 hr

by the agar well diffusion method in Mueller–Hinton Agar (MHA) plates [35-37]. Bacterial inoculum was swabbed on the surface of MHA plates. Wells of 6 mm were made on the MHA plates. 0.2 g of GG-2/Cur-AgNPs hydrogel was poured into the wells. Additionally, 0.2 g of GG gel without any Cur-AgNPs was used as a negative control. Gentamicin 33.5 µM was used as a positive control. The agar plates were incubated at 37 °C for 24 hr. The diameters of the observed zones of inhibition were used as a measure of the antimicrobial efficacy of the GG-2/Cur-AgNPs hydrogels. The experiments were repeated three times for each bacterial strain and average values were recorded. We note that curcumin itself has been proposed as an anti-bacterial [38], however its low water solubility and bioavailability, and poor chemical stability, have limited its utilization in testing, including in this case. Herein curcumin could only be incorporated into GG gels as a surface ligand on the silver nanoparticles and could not be investigated separately.

2.9 Antimicrobial susceptibility

The antimicrobial susceptibility of the GG-2/Cur-AgNPs hydrogel was determined by agar well diffusion as described previously [37,39]. Briefly, bacterial inoculum was swabbed on the surface of Mueller–Hinton Agar (MHA) plates. Then, a hole with a diameter of 6 mm was punched with a sterile tip. After that, 0.1 g of GG-2/Cur-AgNPs hydrogel at concentrations of 0.2, 0.39, 0.78, 1.57, and 3.14 nM of Cur-AgNPs was poured into the well and dried in laminar flow conditions. The agar plates were incubated at 37 °C for 24 hr. After incubation, the no-growth zone or clear zone was measured in millimeters. The results are well-correlated to MIC (minimum inhibitory concentration) since the size of the no-growth zone is determined by the rate of diffusion of the active ingredient through the agar; as the rate reaches its slowest, the MIC is achieved.

3. Results and Discussion

3.1 Preparation of GG-hydrogels

The guar gum-borax hydrogels (GG-hydrogels) were prepared in water at pH 8. First, guar gum was dissolved in DI water and the solution pH was adjusted to 8 by NaOH solution, then borax was used as a cross-linking agent. The borax-initiated gelation mechanism is as follows: (1) The borax was dissolved in water and transformed into borate ions and boric acid, forming boric/borate solution (equation (1) and (2)). (2) The cross-linking proceeds

firstly via monodiol complexation as shown in equation (3), and is then followed by a cross-linking reaction to form the diol-borax complex (equation (4)) to achieve the desired guar-gum borax hydrogels [16,40].

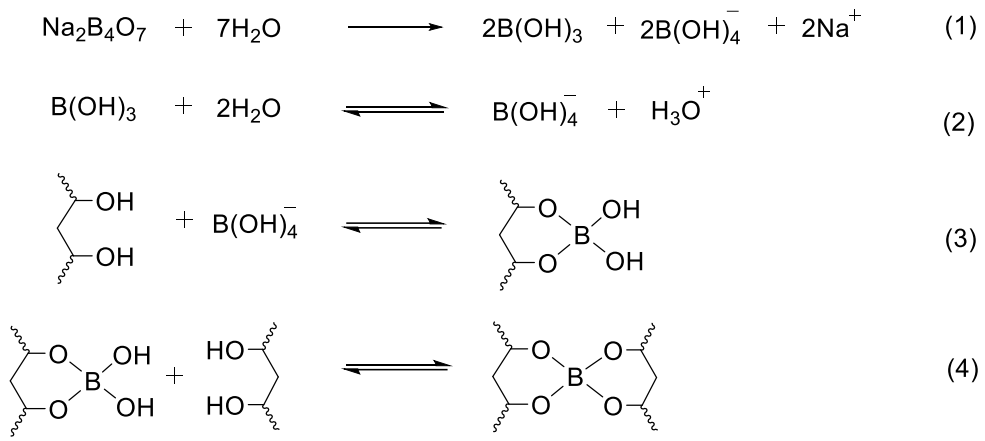

As mentioned earlier a series of four guar gum-borax hydrogels were fabricated with GG:borax weight ratios of 10:1, 5:1, 3.6:1, and 2.5:1, designated here GG-1, GG-2, GG-3 and GG-4, respectively. The different structures of these four hydrogels were investigated by ATR-FTIR spectroscopy (Fig. 1a). In guar gum (GG), the broad peak at 3450 cm^{-1} indicates the presence of O-H stretching vibrations, the peak at 2906 cm^{-1} is characteristic of C-H stretches, and the peaks at 1457 cm^{-1} and 1163 cm^{-1} correspond to C-H bending and C-O-C stretching vibrations, respectively. In the FTIR spectrum of GG-1 to GG-4, the broad peak at 3400 cm^{-1} is drastically reduced. This is attributed to the consumption of hydroxyl groups of the galactomannan backbone to form covalent boronate ester bonds with the borax (Scheme 1). The higher percentage composition of borax, the less prominent the OH stretching peak becomes [16].

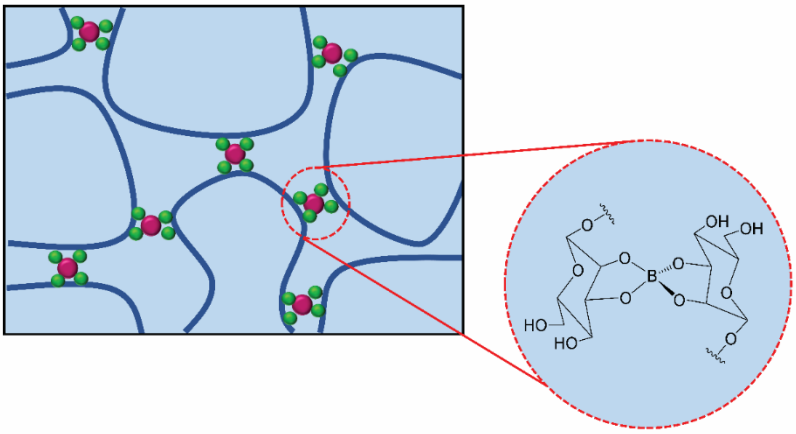

Scheme 1. Schematic illustrations of borax cross-linked guar gum hydrogels

The effect of the density of borax cross-linking on the thermal stability of the GG hydrogels was investigated using thermogravimetric analysis (TGA, Fig. 1b). Weight loss in the first region of the TGA curve spectra (25-250 °C) is assigned to initial moisture loss, while weight loss in the second zone (250 to 350 °C) is attributed to degradation of the main backbone of guar gum. The neat guar gum undergoes 80% weight loss in this zone, but the borax cross-linked gels are much more stable. In the third temperature zone (350-525 °C) degradation of borax-hydrogel hydroxyl bonds can occur. In this zone, the greater wt% borax, and presumably higher cross-linkage density, correlates strongly with stability [16].

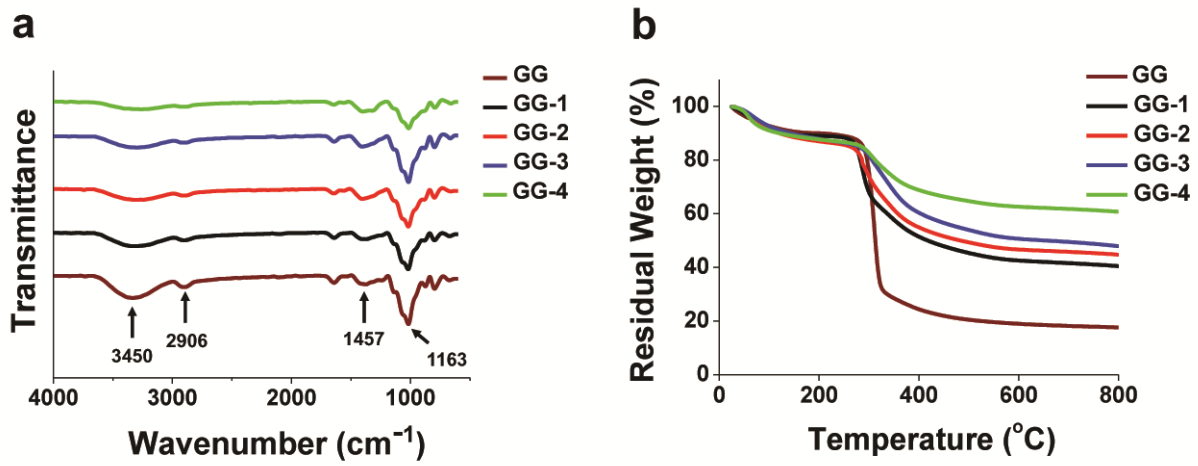

Figure 1. a. ATR-FTIR spectra of hydrogels with different guar gum:borax weight ratios (GG-1 (10:1), GG-2 (5:1), GG-3 (3.6:1) and GG-4 (2.5:1), b. TGA curves of GG, from low cross-linkage density (GG-1) to high cross-linkage density (GG-4).

Despite the guar gum:borax weight ratio being as high as 10:1, and thus reducing the degree of cross-linking and thermal stability, GG-borax hydrogel formation still occurs in all cases (see Fig. 2a). The photographs in Fig. 2b show the injectable nature of the GG-2 hydrogel, it can be easily loaded and dispensed through a 1.2 mm internal diameter needle/syringe (see also discussion further on). As expected, the GG-borax hydrogels are responsive to pH and temperature conditions. Under basic conditions at pH 8.0, the -B-OH groups deprotonate to give -B-O^- groups that quickly react with guar gum via diol complexation, leading to efficient gelation. On the other hand, if -B-O^- groups are protonated to -B-OH by addition of acid at pH 4.0, borax diol complexation is not efficient and de-gelation occurs. However, re-gelation occurs quickly by adding basic solution (Fig. 2c). In addition, the gels break down to form liquids at high temperature but quickly re-gelate when

cooled down (Fig. 2d-f, vials are sealed to avoid evaporation and drying out of the hydrogel at higher temperatures) [41].

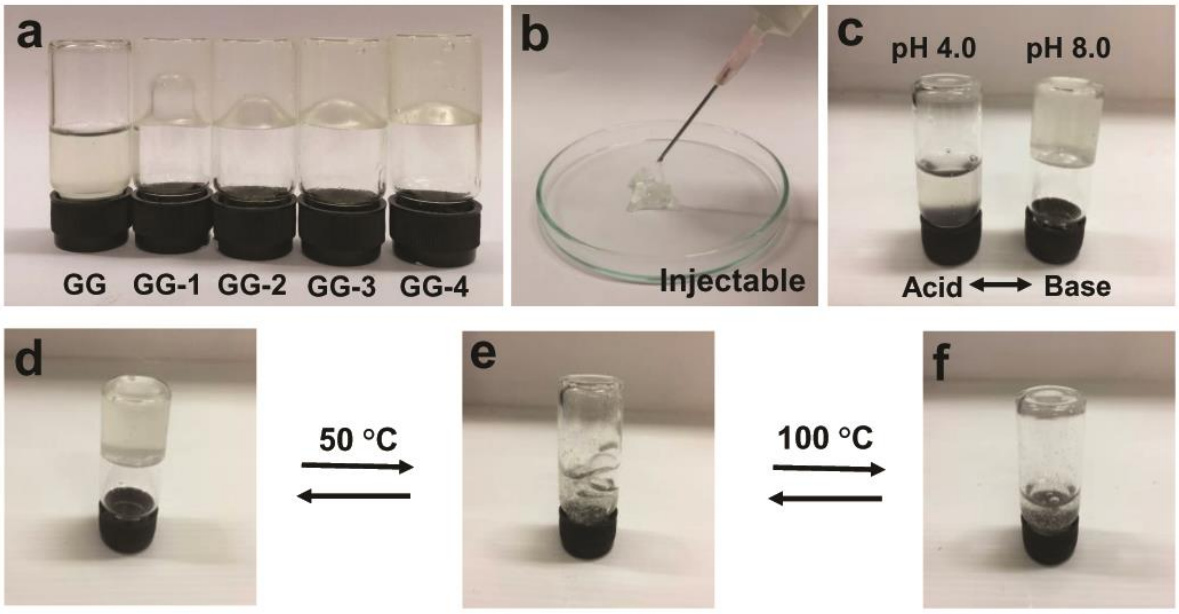

Figure 2. a. The effect of different GG:borax weight ratio on gel formation, from low cross-linker density (GG-1) to high (GG-4), b. Injectability of GG-2 hydrogel (5:1 GG:borax) through a needle with 1.2 mm internal diameter, c-f. reversible GG-2 hydrogel formation in acid (pH 4.0), base (pH 8.0), and in different temperature conditions.

3.2 Morphology analysis

A Leica DVM6 digital microscope was used to study the pore size of the hydrogels as a function of GG:borax weight ratio. Upon increasing the borax content, a decreasing hydrogel pore size was observed (Fig. 3a-d). SEM images of guar gum powder, a guar gum film, and a GG-borax hydrogel, are shown in Fig. 3e-g respectively, allowing further magnification. The guar gum powder shows surface morphology in the form of nodules and flakes. In the case of the guar gum film, a homogenous and compact surface was observed. For the GG-borax hydrogels however there is an outstanding change in morphology, with massive spaces between scaly and fractured material.

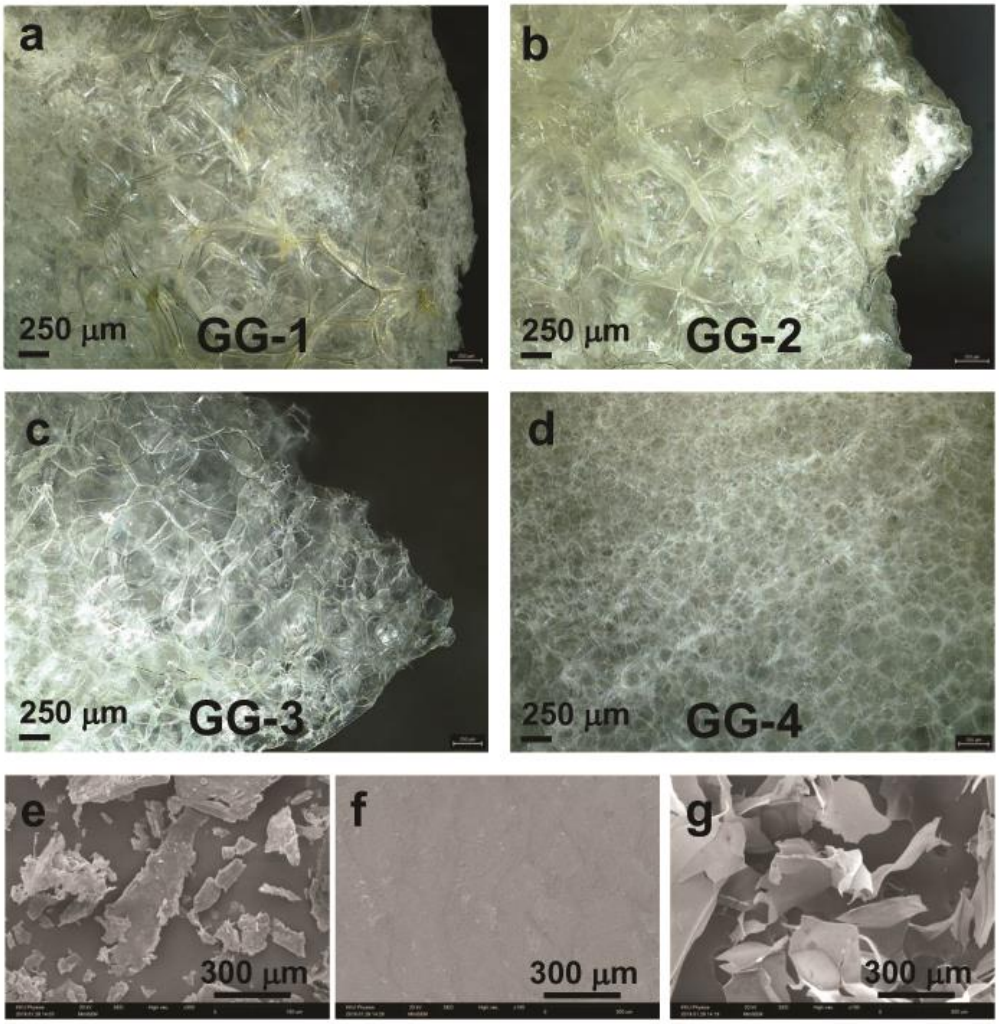

Figure 3. Morphological studies with a Leica DVM6 digital microscopy of hydrogels as a function of GG:borax weight ratio, a. GG-1 hydrogel (10:1 GG:borax), b. GG-2 hydrogel (5:1 GG:borax), c. GG-3 hydrogel (3.6:1 GG:borax), and d. GG-4 hydrogel (2.5:1 GG:borax). Morphological studies with SEM images, e. guar gum powder, f. GG-2 film, and g. GG-2 hydrogel.

3.3 Water absorption

Water uptake by the hydrogels was characterized via their swelling ratio (Fig. 4a). It took about 2 hr soaking for the hydrogels to reach equilibrium size, with GG-4 (maximum borax content) illustrating maximum swelling and GG-1 (minimum borax content) showing the least. Swelling clearly correlates with increased borax composition from 0.05 to 0.2% wt and thus increased cross-linking within the hydrogel as hydrogen bonding was increased as well [16]. Moreover, in the process of gel preparation, the pH solution of guar gum was adjusted

to 8 by adding NaOH then borax with different proportional was added. Eventually, the guar gum film was obtained after drying. Thus, during swelling study, hydroxide ion in the film can repulse the negatively charged of borate ions which increased the network spaces permitting more water to go in.

3.4 Viscosity measurements

Viscosity measurements show an analogous trend (Fig. 4b), with higher wt% borax leading to higher hydrogel viscosity. However while GG-4 (2.5:1 GG:borax) showed the highest viscosity (395 P), the viscosity of GG-1 (10:1 GG:borax) was not much less (382 P).

3.5 Rheological measurements

The rheological properties of the hydrogels were measured by monitoring the storage modulus (G′) and loss modulus (G″) as a function of strain amplitude sweep (γ_0) and frequency sweep at room temperature. G′ and G″ for the hydrogels as a function of weight% borax are shown in Fig 4c. The storage modulus is always larger than the loss modulus, indicating that all the hydrogels exhibit elastic features with a covalent cross-linked network [42,43]. In addition, an increase of the crosslinker density from GG-1 to GG-4 results in a larger storage modulus (G′) and a stiffer gel. No further increase of the modulus is observed above a 3.6:1 GG:borax weight ratio (GG-3). Most interestingly, the hydrogels become stiffer upon the increase of strain in the material, however this smooth increase of both moduli goes through a single turning point at 30% strain amplitude attributed to a breakdown of the cross-linked structure and/or chain scission.

Frequency sweeps were recorded at 1% strain for each of the hydrogels in a range of frequencies from 1 to 100 rad s^{-1}. The results are reported in Fig. 4e. The storage modulus is significantly greater than the loss modulus which suggests that the hydrogels are elastomeric. Furthermore, the moduli are nearly constant up to 70 rad s^{-1}, indicating that the cross-linkage networks of the gels remain unchanged to that point. Above a sweep frequency of 70 rad s^{-1}, the most cross-linked hydrogels, GG-3 and GG-4, degrade indicating change from a cross-linked to an uncross-linked structure ((G″ > G′). However, the degradation of the hydrogels GG-1 and GG-2 with lower cross-linkage density is not observed in the experiment.

3.6 Self-healing properties

The self-healing properties of the hydrogels were evaluated visually by cutting samples into two pieces and dying one of the pieces with Rhodamine 6G to assist visualization. The two blocks were then brought back into contact at room temperature and left for several minutes without temperature changes or light/pressure/chemical stimuli. Each of the various weight% borax guar gum hydrogels showed excellent self-healing, complete within 6 min (an example is shown in Fig. 5 for GG-3). The hydrogel GG-3, with maximum stiffness for minimum borax content (3.6:1 GG:borax weight ratio), was selected for further self-healing experiments with concomitant rheological analyses to monitor qualitatively the self-healing process (Fig. 4d). An original piece of hydrogel GG-3 was cut into two pieces, then the separated blocks brought back immediately into contact. After 6 min, the rheological properties of the self-healed gel were completely recovered, with a similar strain-stiffening and the same strain-at-breakage as uncut GG-3 hydrogel. These results indicate the excellent gelling and self-healing properties of these borax cross-linked hydrogels [44].

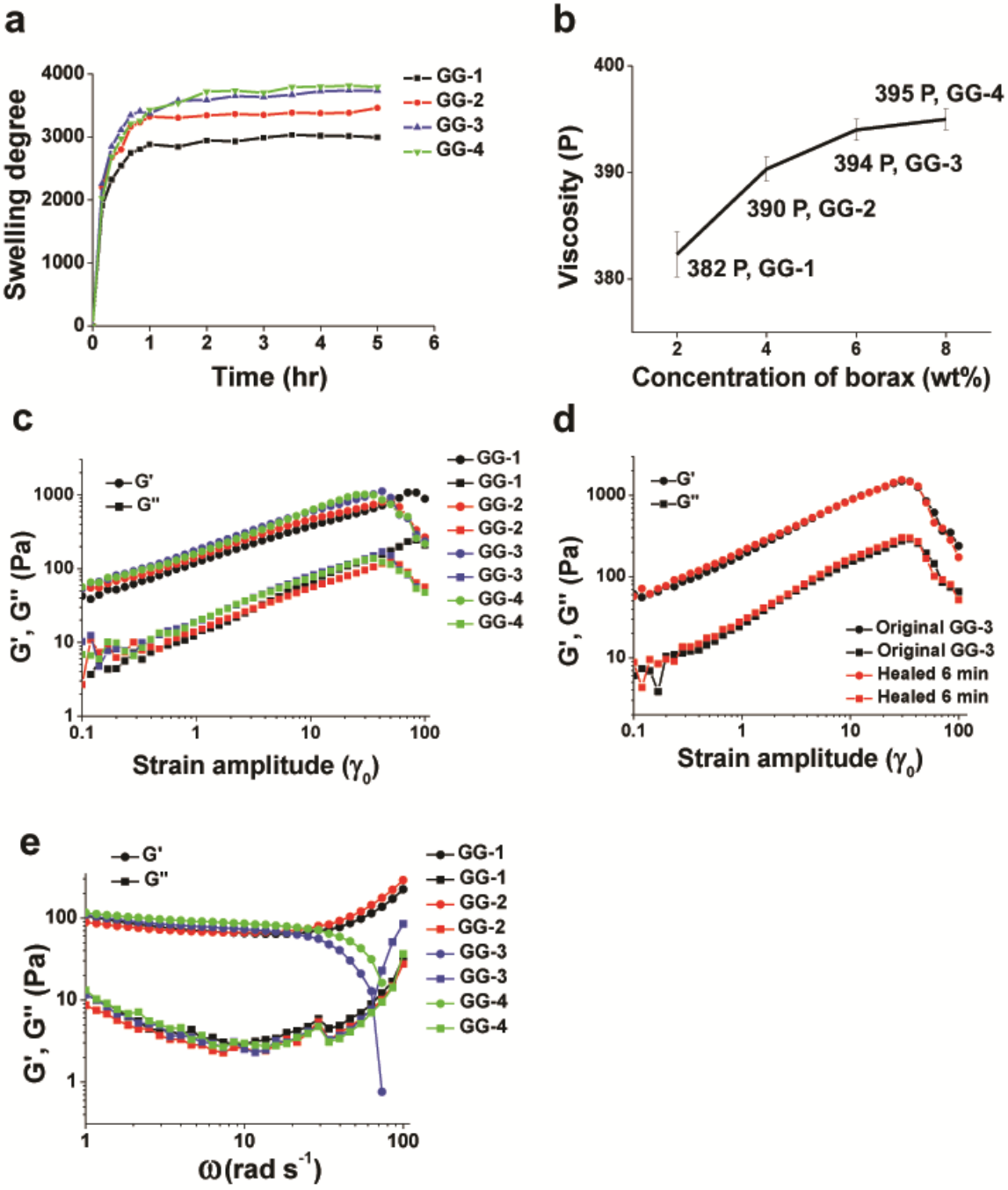

Figure 4. a. Degree of swelling followed over time for GG:borax hydrogels of varying weight ratio, from low cross-linker density (GG-1) to high (GG-4). b. Viscosity of these GG hydrogels c. Storage and loss moduli measured by strain amplitude (γ_0) for all the hydrogels and d. for a cut-and-self-healed GG-3 hydrogel sample compared to an uncut piece. e. Frequency sweep experiments for all the hydrogels at 1% strain amplitude.

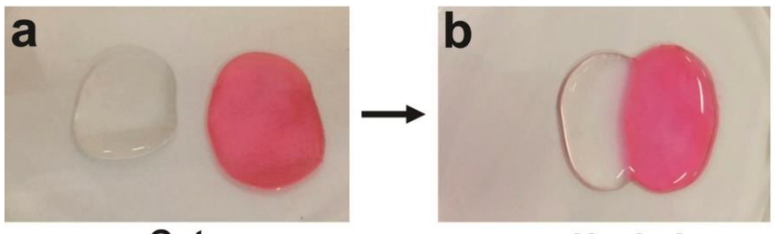

Figure 5. Self-healing properties of the GG-3 hydrogel (3.6:1 GG:borax weight ratio), a. the two pieces resulting from cutting the original hydrogel (the pink piece has been dyed with Rhodamine 6G), b-c. self-healing of the hydrogel upon bringing the two pieces back into contact and d. after 6 minutes, the healed hydrogel could be stretched.

Next, the incorporation of silver nanoparticles into the hydrogels to endow anti-bacterial properties, and an investigation of the injectability of the gels, was undertaken towards developing them as potential biomedical materials. In these studies, outlined below, the 5:1 weight ratio GG:borax hydrogel (GG-2) was focused on as it has a relatively low borax content (hence low toxicity [45]) but was shown to maintain a stable gel structure under high frequency deformations (Fig. 4e) which is an important property for injectable materials. Depending on their stiffness, some injectable gels must be loaded into a syringe as liquid components, only to gel after injection [46]. Here, our hydrogel GG-2 is soft enough to be loaded into a syringe directly and easily expelled through a needle of 1.2 mm internal diameter.

3.7 Nanocomposite of GG-borax hydrogels and silver nanoparticles

Curcumin-stabilized silver nanoparticle (Cur-AgNPs) dispersions were characterized by UV-spectroscopy (Fig. S1) showing a maximum extinction at 407 nm due to localized surface plasmon resonances (SPR) [47, 48]. The size and morphology of the synthesized Cur-AgNPs were studied by transmission electron microscopy (TEM) (Fig. 6a). The results showed the particles to be reasonably monodisperse with a diameter distribution in the range

17.69 ± 3.52 nm (n = 50, Fig. 6b, ImageJ program used for the analysis). The Cur-AgNPs size and size distribution were further characterized using small angle x-ray scattering (SAXS, Fig. 6c,d) to complement the data from TEM. The measured SAXS scattering profile of Cur-AgNPs is shown in Fig. 6d. The intensity profiles are plotted as a function of the scattering vector q, given by $q = 4\pi \sin(\theta/\lambda)$ where θ denotes half the scattering angle and λ is the X-ray wavelength. The scattering profile was well fitted to the unified exponential-power law fit (Fig. 6c) [49]. The fitted parameters were further analyzed by a lognormal size distribution as shown in Fig. 6d (for more detail please see the Experimental Section). The relevant fitted parameters and calculated mean particle radius and standard deviation of the size distribution are shown in Table 1. The result gives a mean radius of 8.84 ± 0.82 nm, which agrees very well with the TEM studies. Finally the Cur-AgNPs particle size was also measured by dynamic light scattering (DLS, Fig. S2) estimating an average particle diameter of 36.1 ± 0.9 nm with a polydispersity index (PDI) of 0.510. This larger estimate may indicate some particle aggregation, or be due to the structure of the stabilizing curcumin layer/hydration sphere in aqueous solution [50].

Table 1 Fitted parameters for the SAXS scattering profile of curcumin-stabilized silver nanoparticles and their calculated mean particle radius and standard deviation compared with the result from TEM.

Sample	SAXS					TEM
	R_g /nm	M	σ	$\langle R \rangle$/nm	SD	R/nm
Cur-AgNPs	1.80	8.80	0.09	8.84	0.82	8.84

Silver nanoparticles have the potential to anchor to bacterial cell walls and then infiltrate them, thereby causing structural changes in the cell membrane, membrane permeability, and cell death [51,52]. In order to incorporate an anti-microbial property to our guar gum hydrogels, aqueous solutions of Cur-AgNPs of different concentrations (0.20, 0.39, 0.78, 1.57, and 3.14 nM, Table S2) were mixed with GG-2 and 4 wt% borax to generate GG-2/Cur-AgNPs hydrogels (designated GG-2/Cur-AgNPs 0.20 nM, GG-2/Cur-AgNPs 0.39 nM, GG-2/Cur-AgNPs 0.78 nM, GG-2/Cur-AgNPs 1.57 nM, and GG-2/Cur-AgNPs 3.14 nM, respectively.). The incorporation of Cur-AgNPs into the hydrogels changes the latter's optical properties, turning them yellow, however the hydrogels still show good structural and self-healing properties (see Fig. S2). The degree of swelling of GG-2/Cur-AgNPs hydrogels

493 increased with increasing concentration of the Cur-AgNPs solution (Fig. 6e). By comparison,
494 the neat GG-2 hydrogel showed lower swelling degree than any of the GG-2/Cur-AgNPs
495 hydrogels. These results indicate that the introduction of curcumin-capped AgNPs, and thus
496 excess OH-functional groups, may lead to more H-bonding with water and improved
497 absorption of water. In addition, these nanocomposite hydrogels still maintain excellent self-
498 healing properties (Fig. S2), and importantly they are also shown to be injectable by syringe
499 (1.2 mm internal diameter needle), a very useful feature in the context of bio-medical
500 applications (Fig. 6f).

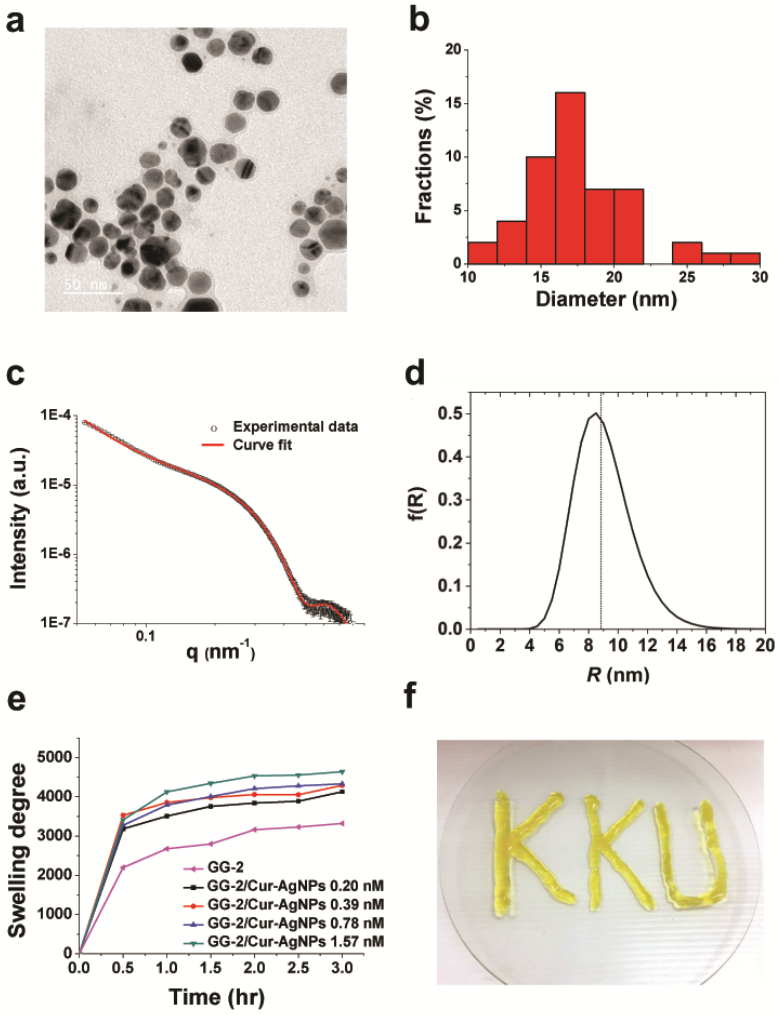

501

502 **Figure 6.** a. TEM image of Cur-AgNPs dispersed on a TEM copper grid (a, scale bar 50 nm),
503 b. A histogram showing diameter distribution of Cur-AgNPs from TEM. c. The SAXS profile
504 (hollow dots) and the unified exponential power-law fit (red solid line) of Cur-AgNPs. d. The
505 lognormal size distribution of Cur-AgNPs obtained from the unified exponential power-law
506 fit (black solid line). The position of the mean radius (8.84 nm) is shown by dotted line. e.
507 Swelling degree of GG-2/Cur-AgNPs hydrogels with various NP concentrations compared to

neat GG-2. f. Picture of the GG-2/Cur-AgNPs hydrogel, syringe-injected to write ‘KKU’ (1.2 mm internal diameter needle).

3.8 Antibacterial activity

The GG-2/Cur-AgNPs hydrogels exhibit strong antimicrobial activity against both Gram-negative bacteria, *E. coli*, *P. aeruginosa* and Gram-positive *S. Aureus*, forming zones of inhibition of diameters 13.5, 13 and 15 mm, respectively (Fig. 7a-c and Table 2). They showed stronger inhibition against Gram-positive bacteria compared to Gram-negative bacteria. The results obtained for antimicrobial activity are impressive and consistent with many earlier reports of plant extract-assisted synthesis of AgNPs [53,54]. The antimicrobial susceptibility of GG-2/Cur-AgNPs hydrogels was determined by agar well diffusion with minimum inhibitory concentration (MIC). The lowest concentration of Cur-AgNPs which inhibits visible growth of a bacterium with a clear zone was determined as the MIC value. After incubation for 24 hr, a zone of inhibition was observed around the agar well (Fig. 7d-f). Bacterial cell growth was inhibited by GG-2/Cur-AgNPs hydrogels at MIC 1.57 nM for *E. coli* and *P. aeruginosa* and at MIC 0.78 nM for *S. aureus*. The hydrogels showed stronger inhibition against Gram-positive bacteria than they did to Gram-negative bacteria.

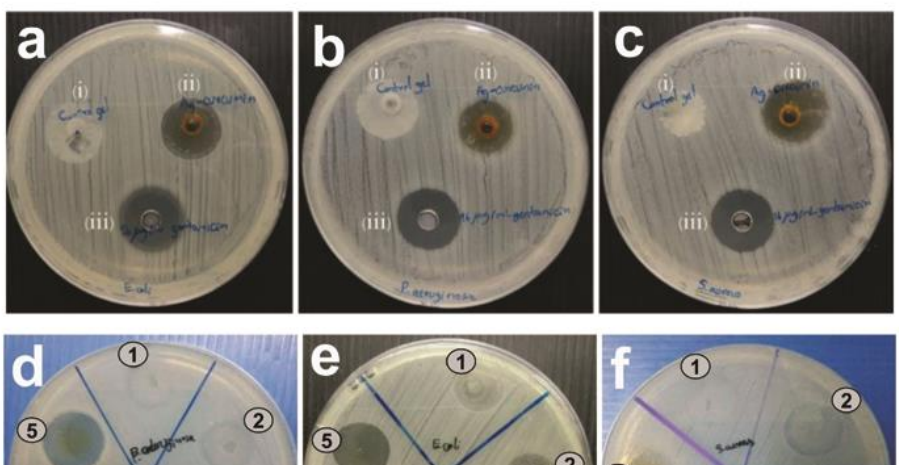

Figure 7. GG-2/Cur-AgNPs and its antimicrobial activity. Position (i) Antimicrobial activity of control gel (without any treatment), position (ii) GG-2/Cur-AgNPs 0.39 nM, and position (iii) gentamicin 33.5 μM against, a. *E.coli*, b. *P.aeruginosa* and c. *S.aureus*. Antimicrobial activity of GG-2/Cur-AgNPs hydrogels at various AgNPs concentrations, 0.2 nM (position 1), 0.39 nM (position 2), 0.78 nM (position 3), 1.57 nM (position 4), and 3.14 nM (position 5), against, d. *P.aeruginosa,* e. *E.coli* and f. *S.aureus*.

Table 2 Zone of inhibition in millimeters (uncertainty ± 0.6 mm) of GG-2/Cur-AgNPs 0.39 nM hydrogels and a standard anti-bacterial, gentamicin, against Gram-negative and Gram-positive bacteria.

Test organism	Zone of inhibition (mm) of GG-2/Cur-AgNPs 0.39 nM	Zone of inhibition (mm) of gentamicin
E.coli	13.5	12.5
P.aeruginosa	13.0	16.0
S.aureus	15.0	14.7

Conclusions

GG hydrogels with high GG:borax weight ratio (10:1 up to 2.5:1) were prepared and characterized by spectroscopy, rheology and microscopy. GG-3 (3.6:1 GG:borax weight ratio) hydrogel exhibits a good compromise between borax content and gel stiffness, whereas

GG-2 (5:1 GG:borax) was more stable to deformation and thus more suitable as an injectable material. Incorporation of curcumin-coated silver nanoparticles into GG-2 not only improved the degree of swelling but also led to the hydrogels exhibiting excellent antimicrobial activity, particularly showing stronger inhibition against Gram-positive bacteria compared to Gram-negative bacteria. Finally, the nanoparticle/hydrogel composite can also be syringe-injected, suggesting these biodegradable materials may have potential in anti-microbial and injectable formulations for biomedical and other industrial applications.

Declaration of interests

We wish to confirm that there are no known conflicts of interest associated with this publication.

Acknowledgement

C.T. was supported by The Science achievement scholarship of Thailand (SAST). W.B. was supported by Development and Promotion of Science and Technology Talents Project (DPST) and S.K. thanks the financial and laboratories support from Faculty of Science, Khon Kaen University and the Center of Excellence for Innovation in Chemistry (PERCH-CIC), Ministry of Higher Education, Science, Research and Innovation. We also thank Dr. Supagorn Rugmai, Dr. Siriwat Soontaranon and Chonthicha Kaewhan at the beamline BL1.3W:SAXS, Synchrotron Light Research Institute (Public Organization, Nakhon Ratchasima) for helpful discussion and setup. J. A. H. acknowledges the Australian Research Council DECRA and Future Fellowship schemes (Grants DE130101300 and FT180100295). We acknowledge Assoc. Prof. Dr. Sayan Saengsuwan and Ubon Ratchathani University for viscosities with fruitful discussion. Finally, we also thank Assist Prof. Dr. Ghislaine Vantomme (Eindhoven University of Technology, Netherland) and Assoc. Prof. Dr. Sittipong Amnuaypanich (Khon Kaen University, Thailand) for discussions on rheology investigation.

References

[1] L. Yu and J. Ding. Injectable hydrogels as unique biomedical materials. Chem. Soc. Rev. 37 (8) (2008) 1473-1481.

[2] L. He, D. Szopinski, Y. Wu, G. A. Luinstra and P. Theato. Toward self-healing hydrogels using one-pot thiol-ene click and borax-diol chemistry. ACS Macro. Lett. 4 (7) (2015) 673-678.

[3] P. Gupta, K. Vermani and S. Garg. Hydrogels: from controlled release to pH-responsive drug delivery. Drug Discov. Today. 7 (10) (2002) 569-579.

[4] J. Tavakoli and Y. Tang. Hydrogel based sensors for biomedical applications: an updated review. Polymers. 9 (8) (2017) 364.

[5] E. Lee and B. Kim. Smart delivery system for cosmetic ingredients using pH-sensitive polymer hydrogel particles. Korean J. Chem. Eng. 28 (6) (2011) 1347-1350.

[6] Z. Q. Lei, H. P. Xiang, Y. J. Yuan, M. Z. Rong and M. Q. Zhang. Room-temperature self-healable and remoldable cross-linked polymer based on the dynamic exchange of disulfide bonds. Chem. Mater. 26 (6) (2014) 2038-2046.

[7] A. K. Blakney, A. B. Little, Y. Jiang and K. A. Woodrow. In vitro-ex vivo correlations between a cell-laden hydrogel and mucosal tissue for screening composite delivery systems. Drug Deliv. 24 (1) (2016) 582-590.

[8] J. L. Drury and D. J. Mooney. Hydrogels for tissue engineering: scaffold design variables and applications. Biomaterials. 24 (24) (2003) 4337-4351.

[9] S. Sharma, A. Kumar, Deepak, R. Kumar, N. K. Rana and B. Koch. Development of a novel chitosan based biocompatible and self-healing hydrogel for controlled release of hydrophilic drug. Int. J. Biol. Macromol. 116 (2018) 37-44.

[10] H. Chen, X. Xin, H. Tan, Y. Jia, T. Zhou, Y. Chen, Z. Ling and X. Hu. Covalently antibacterial alginate-chitosan hydrogel dressing integrated gelatin microspheres containing tetracycline hydrochloride for wound healing. Mater. Sci. Eng. C. 70 (2017) 287-295.

[11] W. Schmolke, N. Perner and S. Seiffert. Dynamically Cross-Linked Polydimethylsiloxane networks with ambient-temperature self-healing. Macromolecules. 48 (24) (2015) 8781-8788.

[12] Z. Wei, J. H. Yang, J. Zhou, F. Xu, M. Zrı´nyi, P. H. Dussault, Y. Osada and Y. M. Chen. Self-healing gels based on constitutional dynamic chemistry and their potential applications. Chem. Soc. Rev. 43 (23) (2014) 8114-8131.

[13] A. B. Ihsan, T. L. Sun, T. Kurokawa, S. N. Karobi, T. Nakajima, T. Nonoyama, C. K. Roy, F. Luo and J. P. Gong. Self-healing behaviors of tough polyampholyte hydrogels. Macromolecules. 49 (11) (2016) 4245-4252.

[14] X. Ye, X. Li, Y. Shen, G. Chang, J. Yang and Z. Gu. Self-healing pH-sensitive cytosine- and guanosine-modified hyaluronic acid hydrogels via hydrogen bonding. 108 (2017) 348-360.

[15] D. R. Bagal-Kestwal, R. M. Kestwal, W.-T. Hsieh and B.-H. Chiang. Chitosan-guar gum-silver nanoparticles hybrid matrix with immobilized enzymes for fabrication of beta-glucan and glucose sensing photometric flow injection system. J. Pharm. Biomed. Anal. 88 (2014) 571-578.

[16] N. Thombare, U. Jha, S. Mishra and M. Z. Siddiqui. Borax cross-linked guar gum hydrogels as potential adsorbents for water purification. Carbohydr. Polym. 168 **(**2017) 274-281.

[17] T. Coviello, P. Matricardi, F. Alhaique, R. Farra, G. Tesei, S. Fiorentino, F. Asaro, G. Milcovich and M. Grass. Guar gum/borax hydrogel: Rheological, low field NMR and release characterizations. Express Polym. Lett. **7** (9) (2013) 733-746.

[18] Y. Sun and Y. Xia. Shape-controlled synthesis of gold and silver nanoparticles. Science. 298 (5601) (2002) 2176-2179.

[19] T. Yamada, K. Fukuhara, K. Matsuoka, H. Minemawari, J. Y. Tsutsumi, N. Fukuda, K. Aoshima, S. Arai, Y. Makita, H. Kubo, T. Enomoto, T. Togashi, M. Kurihara and T. Hasegawa. Nanoparticle chemisorption printing technique for conductive silver patterning with submicron resolution. Nat. Commun. **7** (2016) 11402.

[20] B. Li, X. Wen, R. Li, Z. Wang, P. G. Clem and H. Fan. Stress-induced phase transformation and optical coupling of silver nanoparticle superlattices into mechanically stable nanowires. Nat. Commun. 5 (2014) 4179.

[21] J. R. Morones-Ramirez, J. A. Winkler, C. S. Spina and J. J., Collins. Silver enhances antibiotic activity against gram-negative bacteria. Sci. Transl. Med. 5 (190) (2013) 190ra81.

[22] C. Garcia-Astrain, C. Chen, M. Burón, T. Palomares, A. Eceiza, L. Fruk, M. Á. Corcuera and N. Gabilondo. Biocompatible hydrogel nanocomposite with covalently embedded silver nanoparticles. Biomacromolecules., 16 (4) (2015) 1301-1310.

[23] Y. Rout, S. Behera, A. K. Ojha and P. L. Nayak. Green synthesis of silver nanoparticles using Ocimum sanctum (Tulashi) and study of their antibacterial and antifungal activities. J. Microbiol. Antimicrob. 4 (6) (2012) 103-109.

[24] M. Rai, A. Yadav and A. Gade. Silver nanoparticles as a new generation of antimicrobials. Biotechnol. Adv. 27 (1) (2009) 76-83.

667 [25] R. K. Basniwal, H. S. Buttar, V. K. Jain and N. Jain. Curcumin nanoparticles:
668 preparation, characterization, and antimicrobial study. J. Agric. Food Chem. 59 (5)
669 (2011) 2056-2061.
670 [26] M. H. Kim, H. Park, H. C. Nam, S. R. Park, J. Y. Jung and W. H. Park. Injectable
671 methylcellulose hydrogel containing silver oxide nanoparticles for burn wound healing.
672 Carbohydr. Polym.181 (2018) 579-586.
673 [27] P. Tyagi, M. Singh, H. Kumari, A. Kumari and K. Mukhopadhyay. Bactericidal activity
674 of curcumin I is associated with damaging of bacterial membrane. PloS one. 10 (3)
675 (2015) e0121313.
676 [28] P. J. Manna, T. Mitra, N. Pramanik, V. Kavitha, A. Gnanamani and P. P. Kundu.
677 Potential use of curcumin loaded carboxymethylated guar gum grafted gelatin film for
678 biomedical applications. Int. J. Biol. Macromol. 75 (2015) 437-446.
679 [29] X. X. Yang, C. M. Li and C. Z. Huang. Curcumin modified silver nanoparticles for
680 highly efficient inhibition of respiratory syncytial virus infection. Nanoscale. 8 (5)
681 (2016) 3040-3048.
682 [30] D. Paramelle, A. Sadovoy, S. Gorelik, P. Free, J. Hobley and D. G. Fernig. A rapid
683 method to estimate the concentration of citrate capped silver nanoparticles from UV-
684 visible light spectra. Analyst. 139 (19) (2014) 4855-4861.
685 [31] G. Beaucage. Approximations leading to a unified exponential/power-law approach to
686 small-angle scattering. J. Appl. Crystallogr. 28 (6) (1995) 717-728.
687 [32] I. Breßler, J. Kohlbrecher and A. F. Thünemann. SASfit: a tool for small-angle
688 scattering data analysis using a library of analytical expressions. J. Appl. Crystallogr.
689 48 (5) (2015) 1587-1598.
690 [33] G. Beaucage, H. K. Kammler and S. E. Pratsinis. Particle size distributions from small-
691 angle scattering using global scattering functions. J. Appl. Crystallogr. 37 (4) (2004)
692 523-535.
693 [34] C. Forbes, M. Evans, N. Hastings and B. Peacock, Statistical distributions, 4th ed., John
694 Wiley and Sons Inc., New York, 2011.
695 [35] N. Kannan and S. Subbalaxmi. Green synthesis of silver nanoparticles using Bacillus
696 subtillus IA751 and its antimicrobial activity. Res. J. Nanosci. Nanotechnol. 1 (2)
697 (2011) 87-94.
698 [36] R. Thomas, A. P. Nair, K. R. Soumya, J. Mathew and E. K. Radhakrishnan.
699 Antibacterial activity and synergistic effect of biosynthesized AgNPs with antibiotics

against multidrug-resistant biofilm-forming coagulase-negative staphylococci isolated from clinical samples. Appl. Biochem. Biotechnol. 173 (2) (2014) 449-460.

[37] M. Balouiri, M. Sadiki and S. K. Ibnsouda. Methods for in vitro evaluating antimicrobial activity: A review. J. Pharm. Biomed. Anal. 6 (2) (2016) 71-79.

[38] A. Siviero, E. Gallo, V. Maggini, L. Gori, A. Mugelli, F. Firenzuoli and A. Vannacci. Curcumin, a golden spice with a low bioavailability. J. Herb. Med. 5 (2) (2015) 57-70.

[39] C. Valgas, S. M. D. Souza, E. F. Smânia and A. Smânia Jr. Screening methods to determine antibacterial activity of natural products. Braz. J. Microbiol. 38 (2) (2007) 369-380.

[40] X. Pan, Q. Wang, D. Ning, L. Dai, K. Liu, Y. Ni, L. Chen and L. Huang. Ultraflexible Self-Healing Guar Gum-Glycerol Hydrogel with Injectable, Antifreeze, and Strain-Sensitive Properties. ACS Biomater. Sci. Eng. 4 (9) (2018) 3397-3404.

[41] L. Dai, B. Nadeau, X. An, D. Cheng, Z. Long and Y. Ni. Silver nanoparticles-containing dual-function hydrogels based on a guar gum-sodium borohydride system. Sci. Rep. 6 (2016) 36497.

[42] H. Jiang, G. Zhang, X. Feng, H. Liu, F. Li, M. Wang and H. Li. Room-temperature self-healing tough nanocomposite hydrogel crosslinked by zirconium hydroxide nanoparticles. Compos. Sci. Technol. 140 (2017) 54-62.

[43] J. Qu, X. Zhao, Y. Liang, T. Zhang, P. X. Ma and B. Guo. Antibacterial adhesive injectable hydrogels with rapid self-healing, extensibility and compressibility as wound dressing for joints skin wound healing. Biomaterials. 183 (2018) 185-199.

[44] Y. Deng, I. Hussain, M. Kang, K. Li, F. Yao, S. Liu and G. Fu. Self-recoverable and mechanical-reinforced hydrogel based on hydrophobic interaction with self-healable and conductive properties. Chem. Eng. J. 353 (2018) 900-910.

[45] R. J. Weir and R. S. Fisher. Toxicologic studies on borax and boric acid. Toxicology and applied pharmacology, 23 (1972) 351-364.

[46] E. Piantanida, G. Alonci, A. Bertucci and L. D. Cola. Design of Nanocomposite Injectable Hydrogels for Minimally Invasive Surgery. Acc. Chem. Res. 52 (8) (2019) 2101-2112.

[47] D. Paramelle, A. Sadovoy, S. Gorelik, P. Free, J. Hobley and D. G. Fernig. A rapid method to estimate the concentration of citrate capped silver nanoparticles from UV-visible light spectra. Analyst. 139 (19) (2014) 4855-4861.

[48] N. Agasti and N. K. Kaushik. One pot synthesis of crystalline silver nanoparticles. Am. J. Nanomater. 2 (1) (2014) 4-7.

[49] C. Batista, L. J. Albuquerque, C. A. Ribeiro, C. E. D. Castro, E. G. Miranda, I. L. Nantes, B. L. Albuquerque, M. B. Cardoso and F. C. Giacomelli. Nano-sized silver colloids produced and stabilized by amino-functionalized polymers: polymer structure-nanoparticle features and polymer structure-growth kinetics relationships. J. Braz. Chem. Soc. 28 (9) (2017) 1608-1618.

[50] A. R. Poda, A. J. Bednar, A. J. Kennedy, A. Harmon, M. Hull, D. M. Mitrano, J. F. Ranville and J. Steevens. Characterization of silver nanoparticles using flow-field flow fractionation interfaced to inductively coupled plasma mass spectrometry. J. Chromatogr. A. 1218 (27) (2011) 4219-4225.

[51] L. Ge, Q. Li, M. Wang, J. Ouyang, X. Li and M. M. Xing. Nanosilver particles in medical applications: synthesis, performance, and toxicity. Int. J. Nanomedicine. 9 (2014) 2399-2407.

[52] C. You, C. Han, X. Wang, Y. Zheng, Q. Li, X. Hu and H. Sun. The progress of silver nanoparticles in the antibacterial mechanism, clinical application and cytotoxicity. Mol. Biol. Rep. 39 (9) (2012) 9193-9201.

[53] P. Banerjee, M. Satapathy, A. Mukhopahayay and P. Das. Leaf extract mediated green synthesis of silver nanoparticles from widely available Indian plants: synthesis, characterization, antimicrobial property and toxicity analysis. Bioresour. Bioprocess. 1 (1) (2014) 3.

[54] G. Lakshmanan, A. Sathiyaseelan, P. T. Kalaichelvan and K. Murugesan. Plant-mediated synthesis of silver nanoparticles using fruit extract of Cleome viscosa L.: Assessment of their antibacterial and anticancer activity. Karbala Int. J. Mod. Sci. 4 (1) (2018) 61-68.